Multimodal wide-field two-photon excitation imaging: characterization of the technique for *in vivo* applications

Jae Youn Hwang,[1,2,4] Sebastian Wachsmann-Hogiu,[3] V Krishnan Ramanujan,[1,4] Andreas G. Nowatzyk,[1] Yosef Koronyo,[1] Lali K. Medina-Kauwe,[4,7] Zeev Gross,[5] Harry B. Gray,[6] and Daniel L. Farkas[1,2,4,8,*]

[1]*Minimally Invasive Surgical Technologies Institute and Dept. of Surgery, Cedars-Sinai Medical Center, Los Angeles CA, USA 90048*
[2]*Department of Biomedical Engineering, University of Southern California, Los Angeles CA 90089, USA*
[3]*NSF Center for Biophotonics, Science and Technology, Univ. of California Davis, Sacramento CA 95817, USA, and Department of Pathology and Laboratory Medicine, Univ. of California Davis, Sacramento, CA 9581, USA*
[4]*Department of Biomedical Sciences, Cedars-Sinai Medical Center, Los Angeles, CA 90048, USA*
[5]*Schulich Faculty of Chemistry, Technion-Israel Institute of Technology, Haifa, Israel*
[6]*Beckman Research Institute, California Institute of Technology, Pasadena, CA 91125, USA*
[7]*David Geffen School of Medicine, University of California, Los Angeles, Los Angeles, CA 90095, USA*
[8]*Spectral Molecular Imaging, Inc., Beverly Hills CA 90211*
**dlfarkas@gmail.com*

Abstract: We report fast, non-scanning, wide-field two-photon fluorescence excitation with spectral and lifetime detection for *in vivo* biomedical applications. We determined the optical characteristics of the technique, developed a Gaussian flat-field correction method to reduce artifacts resulting from non-uniform excitation such that contrast is enhanced, and showed that it can be used for *ex vivo* and *in vivo* cellular-level imaging. Two applications were demonstrated: (i) *ex vivo* measurements of beta-amyloid plaques in retinas of transgenic mice, and (ii) *in vivo* imaging of sulfonated gallium(III) corroles injected into tumors. We demonstrate that wide-field two photon fluorescence excitation with flat-field correction provides more penetration depth as well as better contrast and axial resolution than the corresponding one-photon wide field excitation for the same dye. Importantly, when this technique is used together with spectral and fluorescence lifetime detection modules, it offers improved discrimination between fluorescence from molecules of interest and autofluorescence, with higher sensitivity and specificity for *in vivo* applications.

OCIS codes: (180.4315) Microscopy; (110.4234) Imaging systems

References and Links

1. M. Rubart, "Two-photon microscopy of cells and tissue," Circ. Res. **95**(12), 1154–1166 (2004).
2. W. Denk, J. H. Strickler, and W. W. Webb, "Two-photon laser scanning fluorescence microscopy," Science **248**(4951), 73–76 (1990).
3. V. E. Centonze, and J. G. White, "Multiphoton excitation provides optical sections from deeper within scattering specimens than confocal imaging," Biophys. J. **75**(4), 2015–2024 (1998).
4. G. H. Patterson, and D. W. Piston, "Photobleaching in two-photon excitation microscopy," Biophys. J. **78**(4), 2159–2162 (2000).
5. A. Egner, and S. W. Hell, "Time multiplexing and parallelization in multifocal multiphoton microscopy," J. Opt. Soc. Am. A **17**(7), 1192–1201 (2000).
6. Q. T. Nguyen, N. Callamaras, C. Hsieh, and I. Parker, "Construction of a two-photon microscope for video-rate Ca(2+) imaging," Cell Calcium **30**(6), 383–393 (2001).
7. G. J. Brakenhoff, J. Squier, T. Norris, A. C. Bliton, M. H. Wade, and B. Athey, "Real-time two-photon confocal microscopy using a femtosecond, amplified Ti:sapphire system," J. Microsc. **181**(3), 253–259 (1996).

#139427 - $15.00 USD Received 9 Dec 2010; revised 9 Jan 2011; accepted 10 Jan 2011; published 13 Jan 2011

8. V. Nikolenko, B. O. Watson, R. Araya, A. Woodruff, D. S. Peterka, and R. Yuste, "SLM microscopy: scanless two-photon imaging and photostimulation using spatial light modulators," Front. Neural Circuits **2**, 5 (2008).
9. E. Papagiakoumou, V. de Sars, V. Emiliani, and D. Oron, "Temporal focusing with spatially modulated excitation," Opt. Express **17**(7), 5391–5401 (2009).
10. J. Palero, S. I. C. O. Santos, D. Artigas, and P. Loza-Alvarez, "A simple scanless two-photon fluorescence microscope using selective plane illumination," Opt. Express **18**(8), 8491–8498 (2010).
11. S. Wachsmann-Hogiu, J. Y. Hwang, E. Lindsley, and D. L. Farkas, "Wide-field two-photon microscopy: features and advantages for biomedical applications," Prog. Biomed. Opt. Imaging **8**, 1–8 (2007).
12. M. V. Macville, J. A. Van der Laak, E. J. Speel, N. Katzir, Y. Garini, D. Soenksen, G. McNamara, P. C. de Wilde, A. G. Hanselaar, A. H. Hopman, and T. Ried, "Spectral imaging of multi-color chromogenic dyes in pathological specimens," Anal. Cell. Pathol. **22**(3), 133–142 (2001).
13. A. Deniset-Besseau, S. Lévêque-Fort, M. P. Fontaine-Aupart, G. Roger, and P. Georges, "Three-dimensional time-resolved fluorescence imaging by multifocal multiphoton microscopy for a photosensitizer study in living cells," Appl. Opt. **46**(33), 8045–8051 (2007).
14. J. R. Lakowicz, "Emerging applications of fluorescence spectroscopy to cellular imaging: lifetime imaging, metal-ligand probes, multi-photon excitation and light quenching," Scanning Microsc. Suppl. **10**, 213–224 (1996).
15. H. Agadjanian, J. Ma, A. Rentsendorj, V. Valluripalli, J. Y. Hwang, A. Mahammed, D. L. Farkas, H. B. Gray, Z. Gross, and L. K. Medina-Kauwe, "Tumor detection and elimination by a targeted gallium corrole," Proc. Natl. Acad. Sci. U.S.A. **106**(15), 6105–6110 (2009).
16. Z. Okun, L. Kupershmidt, T. Amit, S. Mandel, O. Bar-Am, M. B. Youdim, and Z. Gross, "Manganese corroles prevent intracellular nitration and subsequent death of insulin-producing cells," ACS Chem. Biol. **4**(11), 910–914 (2009).
17. L. Kupershmidt, Z. Okun, T. Amit, S. Mandel, I. Saltsman, A. Mahammed, O. Bar-Am, Z. Gross, and M. B. Youdim, "Metallocorroles as cytoprotective agents against oxidative and nitrative stress in cellular models of neurodegeneration," J. Neurochem. **113**(2), 363–373 (2010).
18. A. Kanamori, M. M. Catrinescu, A. Mahammed, Z. Gross, and L. A. Levin, "Neuroprotection against superoxide anion radical by metallocorroles in cellular and murine models of optic neuropathy," J. Neurochem. **114**(2), 488–498 (2010).
19. M. Koronyo-Hamaoui, Y. Koronyo, A. V. Ljubimov, C. A. Miller, M. K. Ko, K. L. Black, M. Schwartz, and D. L. Farkas, "Identification of amyloid plaques in retinas from Alzheimer's patients and noninvasive *in vivo* optical imaging of retinal plaques in a mouse model," Neuroimage **54**, S204–S217 (2011).
20. H. Agadjanian, J. J. Weaver, A. Mahammed, A. Rentsendorj, S. Bass, J. Kim, I. J. Dmochowski, R. Margalit, H. B. Gray, Z. Gross, and L. K. Medina-Kauwe, "Specific delivery of corroles to cells via noncovalent conjugates with viral proteins," Pharm. Res. **23**(2), 367–377 (2006).
21. S. T. Flock, S. L. Jacques, B. C. Wilson, W. M. Star, and M. J. van Gemert, "Optical properties of Intralipid: a phantom medium for light propagation studies," Lasers Surg. Med. **12**(5), 510–519 (1992).
22. A. Chung, S. Karlan, E. Lindsley, S. Wachsmann-Hogiu, and D. L. Farkas, "*In vivo* cytometry: a spectrum of possibilities," Cytometry A **69A**(3), 142–146 (2006).
23. S. D. Foss, "A method of exponential curve fitting by numerical integration," Biometrics **26**(4), 815–821 (1970).
24. M. E. Dickinson, E. Simbuerger, B. Zimmermann, C. W. Waters, and S. E. Fraser, "Multiphoton excitation spectra in biological samples," J. Biomed. Opt. **8**(3), 329–338 (2003).
25. K. M. Hanson, M. J. Behne, N. P. Barry, T. M. Mauro, E. Gratton, and R. M. Clegg, "Two-photon fluorescence lifetime imaging of the skin stratum corneum pH gradient," Biophys. J. **83**(3), 1682–1690 (2002).
26. B. Rajwa, T. Bernas, H. Acker, J. Dobrucki, and J. P. Robinson, "Single- and two-photon spectral imaging of intrinsic fluorescence of transformed human hepatocytes," Microsc. Res. Tech. **70**(10), 869–879 (2007).
27. D. N. Fittinghoff, P. W. Wiseman, and J. A. Squier, "Widefield multiphoton and temporally decorrelated multifocal multiphoton microscopy," Opt. Express **7**(8), 273–279 (2000).
28. J. C. Jung, A. D. Mehta, E. Aksay, R. Stepnoski, and M. J. Schnitzer, "*In vivo* mammalian brain imaging using one- and two-photon fluorescence microendoscopy," J. Neurophysiol. **92**(5), 3121–3133 (2004).
29. B. A. Flusberg, J. C. Jung, E. D. Cocker, E. P. Anderson, and M. J. Schnitzer, "*In vivo* brain imaging using a portable 3.9 gram two-photon fluorescence microendoscope," Opt. Lett. **30**(17), 2272–2274 (2005).

1. Introduction

Scanning two-photon excited fluorescence microscopy has been widely used as a noninvasive method of advanced microscopy in tissue and live animal imaging, since it can provide axial sectioning capability and allows deeper imaging penetration [1–4]. Various scanning techniques for two-photon imaging including multifocal scanning [5], resonant scanning [6], line-scanning [7], and diffractive optical element-based scanning have been developed in order to monitor fast biological events.

Recently, non-scanning two-photon imaging techniques such as excitation multiplexing by using a spatio-temporal light resonation [8], temporal focusing with spatially modulated

#139427 - $15.00 USD Received 9 Dec 2010; revised 9 Jan 2011; accepted 10 Jan 2011; published 13 Jan 2011

excitation [9], and a simple scanless two-photon excitation based on a selective plane illumination microscopy [10] have been also reported for various biological applications. These studies show that they have a similar axial resolution to scanning two-photon imaging, as well as enable practical optical sectioning in depth-resolved imaging of a particular biological sample.

Two-photon excitation can also be combined, in a multimode setting with fluorescence spectral or lifetime imaging for more demanding applications [11]. To date, spectral and lifetime imaging have been utilized to distinguish and characterize fluorophores targeted to different molecules in intact cells and tissues, yielding an analytical tool with the power of object visualization in biomedical imaging and research [12,13]. Particularly, while imaging *in vivo*, the combination of two-photon excitation with spectral or fluorescence lifetime imaging can enhance capabilities to discriminate between multiple targeted molecules at deeper locations compared to one-photon spectral and fluorescence lifetime imaging [13,14]. However, when a scanning two-photon excitation method is utilized with a non-scanning imaging device, such as an acousto-optical tunable filter (AOTF) and an ultrafast time-gated charge-coupled device (CCD) camera for spectral/fluorescence lifetime detection, synchronization problems may arise, making the approach difficult. In addition, scanning two-photon excited fluorescence imaging is not fit for monitoring fast processes with high magnification *in vivo*, since it is a relatively slow method. Moreover, in live animal imaging, motion artifacts can be easily introduced during scanning two-photon excited fluorescence imaging. To address these limitations, we developed a non-scanning two-photon approach, which allows the combination of two-photon excitation with such non-scanning imaging devices in multi-mode optical imaging for more versatile and faster *in vivo* imaging.

In this paper, we demonstrate the suitability of a non-scanning multimodal optical imaging with wide-field two-photon excitation for *in vivo* applications such as imaging of fluorescent dyes injected into tumors. Here, we employed wide-field two-photon fluorescence excitation and spectral and fluorescence lifetime detection as a non-scanning multimodal optical imaging method. We evaluated the optical characteristics of this simple wide-field two-photon excitation technique, and compared the axial resolving power with that of the one-photon excited fluorescence of the same dye molecules. In investigating the optical characteristics of wide-field two-photon excitation, we examine power, wavelength, numerical aperture, and depth dependence of wide-field two-photon excitation using a fluorescent gallium corrole solution, a sectioned mouse intestine, and a tissue phantom. The particular gallium corrole was chosen because it is both an excellent fluorophore and an anti-tumor agent [15]. This compound, as well as its non-fluorescent iron(III) and manganese(III) analogs are drug candidates for diseases resulting from oxidative/nitrosative stress [16–18]. In addition, *ex vivo* non-scanning wide-field two-photon excitation imaging is performed with an eyecup specimen from an Alzheimer's Disease (AD) transgenic mouse model and images are compared with one photon excitation measurements [19]. Finally, we examine the feasibility of combining wide-field two-photon excitation with multimodal detection (spectral and fluorescence lifetime) for *in vivo* small animal imaging. In this experiment, 100 μM gallium corrole solution and microsphere suspension were injected into tumor regions and subcutaneous regions of an anesthetized mouse, respectively. Depth information and contrast enhancement for these *in vivo* measurements are also discussed.

2. Materials and methods

2.1. Sample preparation

Ex vivo samples. A 16 μm cryostat section of mouse intestine (specifically, the filamentous actin prevalent in the brush border) was stained with Alexa Fluor 568 phalloidin (FluoCells prepared slide #4 (F-24631), Invitrogen) and 50 μM gallium corrole solution [20]. Also, an eyecup specimen from AD transgenic mouse model [Double transgenic mouse harboring the

#139427 - $15.00 USD Received 9 Dec 2010; revised 9 Jan 2011; accepted 10 Jan 2011; published 13 Jan 2011

chimeric mouse/human APP (APPswe) and the mutant human presenilin 1 (PSEN1ΔE9)] was prepared by removing the eyecup anterior part and by staining with curcumin, a natural fluorescent dye (0.1mg/ml) [19].

In vivo samples. In addition, a nude mouse with implanted breast tumors was used for *in vivo* as well as for multimode optical imaging. Furthermore, a concentration of 100 μM gallium corroles (excitation/emission maxima: 425/620nm) and fluorescent microspheres (Constellation fluorescent microsphere, Invitrogen) (excitation/emission maxima: 540/560nm) were prepared with phosphate buffer saline solution (PH 7.4). While the corroles were injected directly in the tumor, the fluorescent microspheres were injected subcutaneously, for comparison.

2.2. Experimental setup for non-scanning multimode optical imaging with wide-field two-photon excitation

The experimental set-up was described elsewhere [11]. Briefly, a polarized femtosecond (100 fs) pulsed tunable laser (MaiTai – Spectra Physics) with 780~990 nm wavelength range, 50-300 mW average power, and 80MHz repetition rate, was utilized for wide-field two-photon excitation. The fs pulsed laser beam is passed through a Faraday rotator, then focused on the back focal plane of the objectives (Nikon 40x, 1.3 NA, oil or Nikon 40x, 0.75 NA, air) through a doublet lens (L1) (Melles Griot, FL200) in order to obtain a quasi-parallel beam that enables wide-field excitation of specimens.

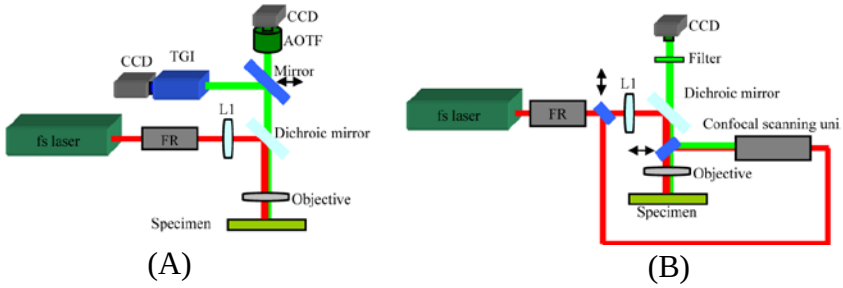

Fig. 1. Schematics of the experimental set-up for wide-field two-photon excitation: (A) multimode optical imaging with wide-field two-photon excitation (B) wide-field two-photon excitation set-up combined with scanning confocal microscopy on an Olympus Fluoview 300 platform. FR: faraday rotator, TGI: time gated intensifier, L1: a doublet lens (focal length: 200mm)

The fluorescence from a specimen, collected by the same objective, passes through a dichroic mirror and either band-pass filters (Chroma Technology, 560 nm ± 8 nm or 630 nm ± 60 nm), a band-sequential spectral selection device (acousto-optical tunable filter (bandwidth (typical): 2.0nm at 600nm), ChromoDynamics Inc.), or a time-gated intensifier (LaVision Picostar, gating: 300ps and step size: 200ps) before being recorded on a cooled CCD (ORCA-ER, Hamamatsu). For one-photon excitation, a Hg lamp incorporated in a commercial microscope (Eclipse TE2000, NIKON) was utilized through excitation filters. Figure 1(A) shows the experimental set-up for wide-field two-photon excitation. Also, a confocal Olympus Fluoview 300 was used for scanning microscopy [Fig. 1(B)] (Olympus IX70, Fluoview).

2.3. Tissue phantom

A tissue phantom was constructed as a test sample that allows for comparison of the contrast and confocality/axial resolution characteristics of wide-field one-photon excited fluorescence, scanning two-photon excited fluorescence, and wide-field two-photon excited fluorescence microscopies [21]. The phantom was composed of a nude mouse skin, a mixed gel (125μM

#139427 - $15.00 USD Received 9 Dec 2010; revised 9 Jan 2011; accepted 10 Jan 2011; published 13 Jan 2011

fluorescein dye, 5% intralipid, and 1% microspheres), and paraffin. After a thin sample of nude mouse skin was put on a slide glass in a chamber, the mixed gel was loaded on the mouse skin. Finally, paraffin was filled in the chamber in order to prevent evaporation from the skin.

2.4. Flat-field correction

Flat-field correction of wide-field two-photon excited fluorescence images was performed using a normalized and inversed Gaussian mask in order to compensate the non-uniform excitation generated by the Gaussian profile of the beam. The Gaussian mask was constructed through the convolution of the original image with a Gaussian function (radius: over 120 pixels) at a focal plane using imaging software we developed (based on ImageJ). The corrected image, R, was obtained by the entry-by-entry product of the original image, O, and the inversed Gaussian mask, M ($R = O. \times M$).

2.5. Spectral/fluorescence lifetime analysis

For spectral imaging and analysis, a classification algorithm based on Euclidean distance measure (Root Sum of Square Error) was utilized. This algorithm is performed with a software package developed in house and previously described elsewhere [22]. For fluorescence lifetime analysis, a single exponential decay fitting method was used to fit the data; it provides the time-constant of a single exponential curve fitted to data on the same pixel in a series of images and generates a fluorescence lifetime image mapped by the time-constants on each pixel [23].

3. Results and discussion

3.1. Optical characteristics of wide-field two-photon excited fluorescence microscopy

In order to validate the wide-field two-photon excitation, we examined the dependence of the fluorescence intensity on the power, wavelength, and numerical aperture of the excitation beam. Measurements on gallium corrole show that the fluorescence intensity increases nonlinearly with the excitation power, suggesting a nonlinear (specifically, two-photon excited) process of fluorescence generation [Fig. 2(A)]. It has a slope of 2.01, in excellent agreement with the typical power dependence of two-photon excitation. In addition, we examined the wavelength dependence of the fluorescence intensity on a sample of a mouse intestine stained with Alexa 568 phalloidin. Fluorescence intensities were measured on images recorded at different excitation wavelengths (780-910 nm, step: 10nm). The excitation wavelength dependence is very similar to that reported previously for two-photon excitation [24]. In addition, we examined possible photobleaching effects, to confirm the accuracy of the result. We found negligible (0.03%) photobleaching during the experiment [intensity (Arbitrary Unit): 1541 before to 1497 after]. Finally, the dependence of the fluorescence intensity on the numerical aperture of the objective lens was investigated with a sample consisting of a mouse intestine specimen. Figure 2(C) shows that the fitting curve displays a nonlinearity (4th order) of the wide-field two-photon excitation-induced signal intensity vs. numerical aperture. The field of view (FOV) has not changed significantly by a numerical aperture but it changed proportionally to the magnification of objectives. Here, the fluorescence intensity obtained with the 40x (NA: 1.30) objective is four times higher than that obtained with the 40x (NA: 0.75) objective. Altogether, these results suggest that the wide-field two-photon excitation has almost similar characteristics to typical two-photon scanning excitation, thus indicating that the fluorescence signal is indeed generated from two-photon excitation.

#139427 - $15.00 USD Received 9 Dec 2010; revised 9 Jan 2011; accepted 10 Jan 2011; published 13 Jan 2011

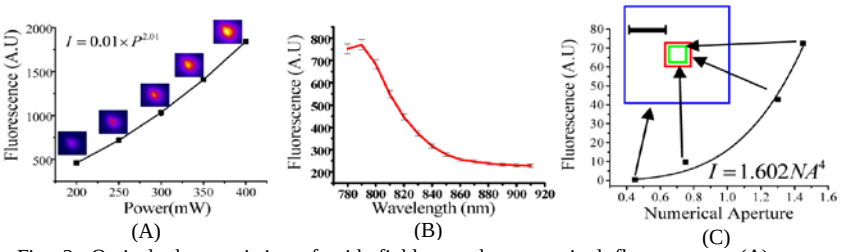

(A) (B) (C)

Fig. 2. Optical characteristics of wide-field two-photon excited fluorescence: (A) power dependence of the fluorescence of gallium corroles (50μM) (B) fluorescence intensity versus wavelength of the mouse intestine stained with Alexa 568 phalloidin [power density: 64μW/μm^2, ex: 780-910 nm (step: 10 nm), em: 620 ± 60 nm, and a 40x air objective]. (C) fluorescence intensity versus numerical aperture of the objective lens [ex: 780 nm, power density: 64μW/μm^2, 10x (NA: 0.45, FOV: 256 μm x 244 μm), 40x (NA: 0.75, FOV: 64 μm x 61 μm), 40x (NA: 1.30, FOV: 64 μm x 61 μm), and 60x (NA: 1.45, FOV: 43 μm x 41 μm)]. The rectangles represent the size of FOV.

3.2. Sectioning capability of wide-field two-photon microscopy

One important advantage of scanning two-photon microscopy is the intrinsic confocality due to the nonlinear nature of the excitation process. However, for wide-field excitation, the numerical aperture of the excitation beam is significantly lower and one would expect a loss in confocality. Here we investigated the sectioning capability of wide-field two-photon microscopy and compared it with its scanning counterpart and with wide-field one-photon imaging. We performed measurements on the tissue phantom described previously and compared 52 images recorded within 0~153 μm from the surface, with a step size of 3 μm.

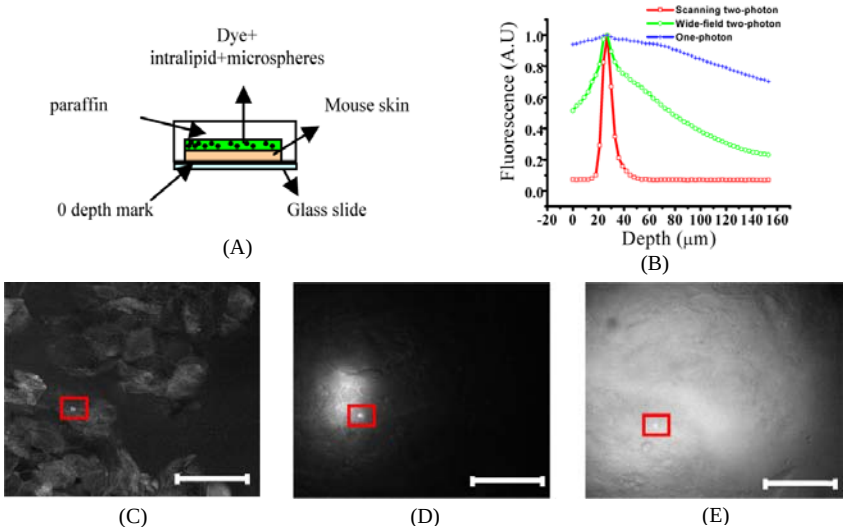

(A) (B)

(C) (D) (E)

Fig. 3. Comparisons of the depth dependence in scanning two-photon, wide-field two-photon, and wide-field one-photon excitation for a tissue phantom: (A) schematic of the tissue phantom (B) Intensity profiles over the selected regions (microspheres) along the axial (depth) coordinate (C) Scanning two-photon excited fluorescence image obtained with a fs pulsed laser light source at 780nm. (D) Wide-field two-photon excited fluorescence image without Gaussian correction (excitation with a fs laser at 780 nm,) (E) Wide-field one-photon excited fluorescence image (excitation at 488 ± 30 nm). The scale bar is 50μm.

Figures 3(C), (D), and (E) show the scanning two-photon, wide-field two-photon, and one-photon excited fluorescence image (the same focal plane), respectively. In the figure, the intensity profiles of the microsphere selected by a solid rectangle were examined along a

#139427 - $15.00 USD Received 9 Dec 2010; revised 9 Jan 2011; accepted 10 Jan 2011; published 13 Jan 2011

depth for contrast comparison. Figure 3(B) shows the profiles along the depth (z-axis). This data shows that the full width at half maximum of the intensity profile in the scanning two-photon excitation is narrowest (approximately 10 μm), while in the wide-field two-photon excitation is estimated at 60 μm. This is significantly smaller than that of wide-field one-photon excitation, which was measured to be slightly larger than 160 μm. Generally, the full width at half maximum in the intensity profiles along a depth indicates intermediate axial resolution and contrast. Thus, these results suggest that the sectioning capability and its image contrast is better for wide-field two-photon than wide-field one-photon, though worse than scanning two-photon excitation. It is important to note that the sectioning capability depends on the L1 coupling lens (doublet lens, focal length: 200mm): the shorter focal length of L1 provides a larger field of view and less sectioning capability, and a compromise can be selected depending on experimental priorities. Furthermore, the axial sectioning capability of this method could be improved via spinning disks or deconvolution methods.

3.3. Ex vivo applications: imaging of a retinal specimen of Alzheimer's Disease (AD) from a transgenic mouse model

We tested the ability of this method to detect labeled beta-amyloid plaques *ex vivo*. We used specimens from an AD transgenic mouse model that expresses beta-amyloid plaques in the retina. The samples were stained with curcumin to specifically label beta-amyloid plaques [19], and wide-field two-photon images were obtained and compared with wide-field one-photon images. Figures 4(B) and (C) show the uncorrected and Gaussian-corrected, wide-field two-photon excited fluorescence images, respectively. More plaques are clearly observed in Fig. 4(B) and (C) than in the one-photon excited fluorescence image. Furthermore and as before, the Gaussian-corrected image shows better contrast than the uncorrected one, and the background due to non-uniform illumination is removed, as demonstrated by the intensity profiles across the corrected image along the dotted line (a') [Fig. 4(D)]. It is important to mention that the use of a Gaussian mask generated from the original image rather than using the mathematics equation of a Gaussian beam (as previously reported by Fittinghoff et al (14)) has some advantages as it accounts for unknown distortions created inherently by the excitation beam and coupling optics. Altogether, the results suggest that wide-field two-photon excitation with Gaussian correction provides better contrast than one photon imaging.

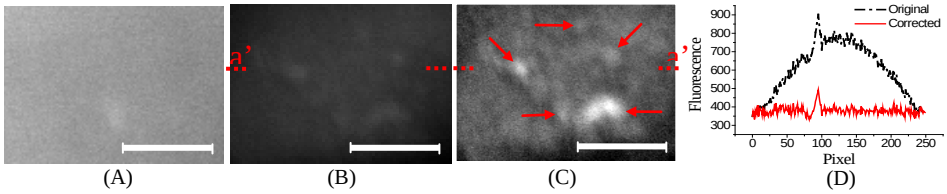

Fig. 4. Wide-field one photon and wide-field two-photon imaging of an eye specimen from an AD transgenic mouse model: (A) One photon excited fluorescence image (excitation at 560 nm, emission at 630 nm) (B) Wide-field two-photon excited fluorescence image without Gaussian correction (excitation at 830nm, emission at 630nm) (C) Gaussian corrected wide-field two-photon excited fluorescence image (scale bar: 25μm): The plaques can be visualized and appear as brighter white signal compared to the background; the arrows indicate plaques (D) Profile of cross-sections of the original and the corrected image along a horizontal line (a').

3.4. In vivo applications: multimode optical imaging of nude mouse bearing gallium corroles and microspheres

We performed multimodal (spectral and fluorescence lifetime) optical imaging of a small animal *in vivo* with wide-field two-photon on a HER2 + tumor-bearing mouse model. 100 μM gallium corrole solution and microsphere suspension were injected into the tumor regions and subcutaneous regions of the anesthetized mouse respectively [Fig. 5(A)]. In order to examine

#139427 - $15.00 USD Received 9 Dec 2010; revised 9 Jan 2011; accepted 10 Jan 2011; published 13 Jan 2011

the penetration depth of the technique and compare it with one-photon excitation, we recorded 40 one-photon and wide-field two-photon excited fluorescence images around the injection region of the microsphere suspension at different depths (0 - 20 μm, step: 0.5 μm) beneath the skin. In Fig. 5(B) and (C), while several microspheres (the arrows indicate microspheres) are clearly visible in wide-field two-photon excited fluorescence image at 13.5 μm and 17 μm [Fig. 5(C)], they are not easily detectable in the one-photon excited fluorescence images at those focal planes [Fig. 5(B)]. Figure 5(B) and (C) here show only images at four focal planes (10 μm, 10.5 μm, 13.5 μm, and 17 μm) beneath the skin. Generally, two-photon excitation allows imaging at higher depth than one-photon excitation, due to reduced absorption and scattering at longer wavelengths. This is confirmed here for *in vivo* measurements of fluorescence excited in a wide-field two-photon configuration.

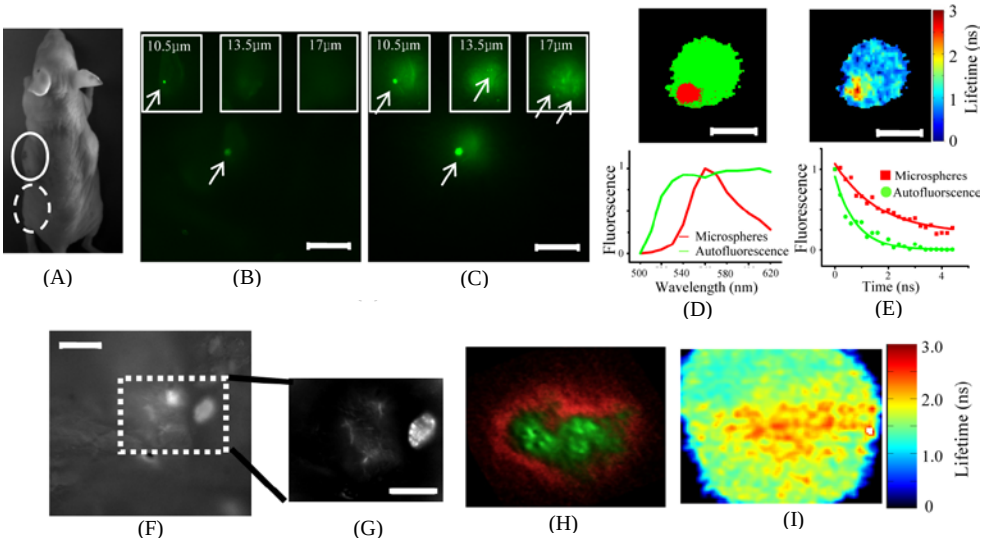

Fig. 5. Multimodal optical imaging with wide-field two-photon excitation of a nude mouse: (A) A nude mouse: solid circle indicates the corroles-injected tumor region; the dotted circle indicates the microsphere solution injected region. (B) One-photon and (C) wide-field two-photon excited fluorescence images (before Gaussian-correction) of microspheres at the indicated different depths (center: 10 μm, insets: 10.5 μm, 13.5 μm, and 17 μm) beneath the skin around the regions selected by the dotted circle. The insets are the depth-resolved images. The arrows indicate microspheres. (D) Spectral and (E) fluorescence lifetime images of a microsphere obtained with wide-field two-photon excitation. The spectral and fluorescence lifetime images were obtained at the same depth (10 μm) and field of view with Fig. 5(C) (center). (F) One-photon (excitation 425nm and emission 620nm, field of view: 75 μm x 75 μm) and (G) wide-field two-photon (excitation 800nm and emission 620nm) image around the tumor regions (indicated by the solid circle), indication the presence and spatial distribution of corroles. (H) Spectral classification and (I) fluorescence lifetime images of corroles.

In addition, two distinct topologically resolved spectroscopic modalities, spectral and fluorescence lifetime imaging, were combined with wide-field two-photon excitation for improved specificity of detection of corroles and fluorescent microspheres. For spectral classification, we selected two spectral signatures shown in the Fig. 5(D) (a lower panel). The spectral signature of microspheres exhibits a peak at 560 nm and it is much narrower than the autofluorescence spectrum. Figure 5(D) (an upper panel) shows the classified image based on the selected signatures. Here, the red color represents the fluorescence of microspheres and the green color represents tissue autofluorescence. Fluorescence lifetime imaging of microspheres can also be used to discriminate between microspheres and intrinsic fluorophores. While the fluorescence lifetime of microspheres in this image [Fig. 5(E)] appears to be approximately 1.8~2.3 ns, the autofluorescence lifetime is slower at less than 1.2

#139427 - $15.00 USD Received 9 Dec 2010; revised 9 Jan 2011; accepted 10 Jan 2011; published 13 Jan 2011

ns. The graph (a lower panel) in Fig. 5(E) shows that the intensity of fluorescence from microspheres and autofluorescence decays along the time (0~4.2 ns). The exponential decay coefficients of the fluorescence and autofluorescence were measured to be 2.15 ns and 0.78 ns, respectively. In the fluorescence lifetime analysis, the signals were thresholded (over 1000 in intensity), since the lifetime decays can be incorrectly interpreted as shorter than they are with low signals. Additional measurements were performed in and around the tumor region which was injected with corroles. We observed that the thin blood vessels around tumor regions are more clearly shown in the Gaussian corrected wide-field two-photon image [Fig. 5(G)] than in the one-photon excited fluorescence image [Fig. 5(F)]. Finally, we can discriminate between corroles and other fluorescent molecules using spectral [Fig. 5(H)] and florescence lifetime imaging [Fig. 5(I)]. In the spectral image, while the green color represents corroles, the red color represents autofluorescence [Fig. 5(H)]. This shows clearly that corroles are localized in the tumor, and allows for separation from the autofluorescence background. Moreover, the fluorescence lifetime imaging also allows us to discriminate between them by the difference in fluorescence lifetime values. The fluorescence lifetime of corroles around tumor regions is measured at approximately 1.9ns~2.3ns [Fig. 5(I)], which is longer than autofluorescence lifetime measured in adjacent regions. In previous studies, the fluorescence lifetimes of gallium corroles are longer in acidic environment than in alkali environment, and are higher in tumors than in normal tissues. The fluorescence lifetime values shown here show good agreement with the values in our previous study [Hwang, J.Y. et al, submitted for publication].

4. Conclusion

We demonstrated here for the first time the suitability of wide-field two-photon excitation and non-scanning *multimodal* imaging (spectral and fluorescence lifetime) for *in vivo* small animal imaging. As a non-scanning method, it can be relatively simpler and faster than comparable scanning methods, while simultaneously it can provide better contrast and more penetration depth than wide-field one-photon imaging. In addition, it may be less susceptible to animal motion-generated artifacts, as the image is recorded in one shot.

Our results also demonstrate the ability to discriminate, *in vivo*, between different fluorescent molecules and the possibility of acquiring diverse, complementary information such as quantitative/environmental data simultaneously [25,26].

However, we should note that wide-field two-photon excited fluorescence imaging does not preserve *all* the advantages of scanning two-photon excited fluorescence imaging. In particular, the axial sectioning capability is somewhat reduced since the out-of-focus light does not decrease significantly as illumination occurs with a quasi-parallel geometry [10,27]. In addition, while the penetration depth of near infrared light is still larger than of visible light, image degradation due to photon migration (of emitted photons) may play a significant role when imaging at the larger depth is performed. However, in spite of some disadvantages, employing this method overcomes the inherent shortcomings of scanning two-photon microscopy (low speed and need for scanning), and allows investigation and analysis of molecules of interest *in vivo* in a multimodal optical imaging setting, without the need for scanning. Here, the loss in image quality and penetration depth is a minor sacrifice compared to the gains made in the versatility for small animals *in vivo*, as this simple method can be employed in situations such as real-time imaging of small animals where two-photon microscopy was previously unavailable without complications, compromises or very sophisticated and thus scarcely available scanning [28,29].

Acknowledgments

Partial support from the U.S. Navy Bureau of Medicine and Surgery is gratefully acknowledged. Work at Caltech was supported by a CIT-COH initiative grant.

#139427 - $15.00 USD Received 9 Dec 2010; revised 9 Jan 2011; accepted 10 Jan 2011; published 13 Jan 2011